available at www.sciencedirect.com

ScienceDirect

journal homepage: www.elsevier.com/locate/chnjc

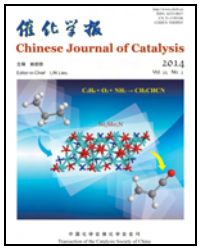

Article

Cobalt-based catalysts derived from cobalt carbonyl clusters for Fischer-Tropsch synthesis

Xuefen Li [a], Fenghua Bai [b], Haiquan Su [a,b,*]

[a] College of Life Sciences, Inner Mongolia University, Hohhot 010021, Inner Mongolia, China
[b] School of Chemistry and Chemical Engineering, Inner Mongolia University, Hohhot 010021, Inner Mongolia, China

ARTICLE INFO

Article history:
Received 2 September 2013
Accepted 22 November 2013
Published 20 March 2014

Keywords:
Cobalt carbonyl cluster
Fischer-Tropsch synthesis
Precursor
Impregnation

ABSTRACT

Co catalysts supported on γ-Al_2O_3 were prepared using $Co_2(CO)_6HCCCOOH$, $Co_3(CO)_9CCH_2COOH$, and $Co_4(CO)_{10}HCCCOOH$ as precursors. $Co(NO_3)_2$ was used as the precursor for preparing the reference catalyst. The results of Fischer-Tropsch synthesis tests and characterization by transmission electron microscopy, NH_3 temperature-programmed desorption, and infrared showed that the different precursors have significant effects on the dispersion of the Co, which affect their catalytic behavior. CO conversion and C_{5+} selectivity over these catalysts prepared from different precursors decreased in the order $Co_3(CO)_9CCH_2COOH$ > $Co_2(CO)_6HCCCOOH$ > $Co_4(CO)_{10}HCCCOOH$ > $Co(NO_3)_2$.

1. Introduction

Fischer-Tropsch (F-T) synthesis is one of the most promising alternative routes for converting natural gas and coal into liquid fuels. Cobalt-based catalysts are the preferred catalyst due to high activity and selectivity toward linear hydrocarbons, and low activity for the water-gas shift (WGS) reaction[1]. It is known that the product distribution from F-T synthesis usually follows the Anderson-Schultz-Flory (ASF) law, and it is difficult to obtain specific hydrocarbons in high selectivity from F-T synthesis. Thus, it is a critical issue to rationally design new Co-based catalysts with enhanced higher liquid hydrocarbon selectivity in F-T synthesis [2,3]. Many studies showed that the cobalt sources had a significant effect on the metal-support interaction, reduction properties and dispersion, and the activity and selectivity of the catalysts prepared by impregnation [4,5]. $Co(NO_3)_2$ is often used as the Co salt in the catalyst preparation, however, other compounds such as $Co_2(CO)_8$, $Co_4(CO)_{12}$, Co-EDTA, $Co(acac)_3$, and $Co(CH_3COO)_2$ can also be used. Kraum et al. [6] systematically studied the correlation between catalytic activity and the cobalt source for TiO_2-supported catalysts using different Co precursors, and found that the catalytic activity decreased in the order $Co(COO)_2$ > $Co(CH_3COO)_2$ > $Co(acac)_3$ > $Co(NO_3)_2$ > Co-EDTA > $Co(acac)_2$. Niemela et al. [7] reported on the performance of 5% Co/SiO_2 catalysts prepared from different cobalt sources for F-T synthesis. They found that the dispersion of the active components followed the order of $Co_2(CO)_8$ > $Co_4(CO)_{12}$ >> $Co(NO_3)_2$. Compared to the traditional Co catalyst, cobalt carbonyl clusters can provide zero valent metal particles and do not need to be reduced at high temperature. Moreover, multimetallic carbonyl clusters have a potential more efficient metal synergy. In this work, we prepared a serious of Co-based catalysts using carbonyl clusters as the cobalt precursors. Their catalytic performance for F-T synthesis was investigated, and was also compared with the catalyst prepared using $Co(NO_3)_2$.

* Corresponding author. Tel/Fax: +86-471-4992981; E-mail: haiquansu@yahoo.com
This work was supported by the National Natural Science Foundation of China (21061008) and the Key Grant of Inner Mongolia Natural Science Foundation (2010ZD01).
DOI: 10.1016/S1872-2067(12)60757-8 | http://www.sciencedirect.com/science/journal/18722067 | Chin. J. Catal., Vol. 35, No. 3, March 2014

2. Experimental

2.1. Materials

$Co(NO_3)_2{\cdot}6H_2O$ was purchased from a domestic supplier. γ-Al_2O_3 was purchased from Alfa Aesar. $Co_4(CO)_{10}HCCCOOH$ and $Co_2(CO)_6HCCCOOH$ were prepared according to published procedures [8]. The molecular structures are shown in Fig. 1. $Co_3(CO)_9CCH_2COOH$ was obtained by the reaction of $(CO)_{10}Co_4HCCCOOH$ and $Eu(OOCCF_3)_3$ dissolved in freshly distilled tetrahydrofuran (THF). The crystal structural parameters and data are given in Table 1. Selected bond lengths and angles are given in Table 2. The structure and the atom numbering scheme is shown in Fig. 1(c). X-ray single crystal analysis revealed $Co_3(CO)_9CCH_2COOH$ is a triclinic system with the centro-symmetrical space group P-ī (see Table 1).

2.2. Catalyst preparation

The γ-Al_2O_3 support was calcined at 500 °C for 10 h to dehydroxylate the surface prior to use. The Co catalysts were prepared by conventional incipient wetness impregnation of γ-Al_2O_3 (40–60 mesh) using THF solution of $Co_2(CO)_6HCCCOOH$, $Co_3(CO)_9CCH_2COOH$, or $Co_4(CO)_{10}HCCCOOH$ under N_2 atmosphere. Excess solvent was removed by N_2 flow. The solids obtained were dried in N_2 atmosphere for 24 h at room temperature, and named as Co_n/γ-Al_2O_3 (n = 2, 3, 4; the same below). The Co(N)/γ-Al_2O_3 catalyst was prepared by incipient wetness impregnation with $Co(NO_3)_2$ and dried in air at 120 °C for 12 h. Then, the sample was calcined in air at 350 °C for 6 h. Co contents in these samples were 10 wt%.

2.3. Catalyst pretreatment

The catalysts with the two types of precursors were pretreated under different pretreatment conditions. The temperature-programmed hydrogen reduction experiment of Co(N)/γ-Al_2O_3 catalyst showed the typical reduction behavior of Co/Al_2O_3 with the peak at 347 °C attributed to the reduction of bulk Co_3O_4 ($Co^{3+}\rightarrow Co^{2+}$) in the catalyst and the high temperature peak (396–470 °C) attributed to the reduction of $Co^{2+}\rightarrow Co^0$ [9,10]. Since the Co_3O_4 species can interact with Al_2O_3 at high temperature to form the irreducible $CoAlO_4$ species [11], the Co(N)/γ-Al_2O_3 catalyst was reduced at 400 °C in a hydrogen flow. However, the Co_n/Al_2O_3 catalysts with zero valent cobalt were only flushed with H_2 flow at 200 °C.

Table 1
Crystal and structural data of $Co_3(CO)_9CCH_2COOH$.

Empirical formula	$C_{12}H_3Co_3O_{11}$
Formula weight	499.76
Crystal system	Triclinic
Space group	P-ī
Unit cell dimensions	a (Å) = 8.2074(7) b (Å) = 13.5852(12) c (Å) = 15.9065(14) α (°) = 95.6430(10) β (°) = 101.035(2) γ (°) = 92.4500(10)
Z	4
Dcalc (g/cm^3)	1.917
Absorption coefficient (mm^{-1})	2.898
F(000)	972
Crystal size	0.31 mm × 0.12 mm × 0.10 mm
θ range for data collection (°)	1.51–25.02
Reflections collected / unique	8900 / 5962 [R(int) = 0.0301]
Absorption correction	Semi-empirical from equivalents
Max. and min. transmission	0.7604 and 0.4669
Refinement method	Full-matrix least-squares on F^2
Data/restraints/parameters	5962/0/469
Goodness-of-fit on F^2	1.018
Final R indice [I>2sigma(I)]	R_1 = 0.0556, ωR_2 = 0.1470
R indice (all data)	R_1 = 0.0885, ωR_2 = 0.1787
Largest diff. peak and hole (e Å^{-3})	1.826 and −0.585
Temperature (°C)	25(2)

2.4. Catalytic activity test

F-T synthesis was carried out in a fixed-bed stainless steel reactor (ϕ 18 mm × 700 mm). The catalyst (4 g) was loaded into the reactor, flushed with high purity H_2 at 200 °C ($Co(NO_3)_2/Al_2O_3$ at 400 °C) for 10 h, and then the catalyst was slowly cooled to 180 °C under H_2 flow. The inlet gas was switched to syngas (H_2/CO = 2), the pressure was increased to 2.0 MPa and the reactor temperature was raised to 220 °C in 1 h. Ar was used as an internal standard for the calculation of CO conversion. The gas hourly space velocity (GHSV) was kept constant at 500 h^{-1}. The outlet gases containing H_2, CO, CH_4, and CO_2 were analyzed by online gas chromatography on a Shimadzu GC-8A equipped with a TDX-01 carbon molecular sieve column and a TCD detector. Hydrocarbon products with carbon

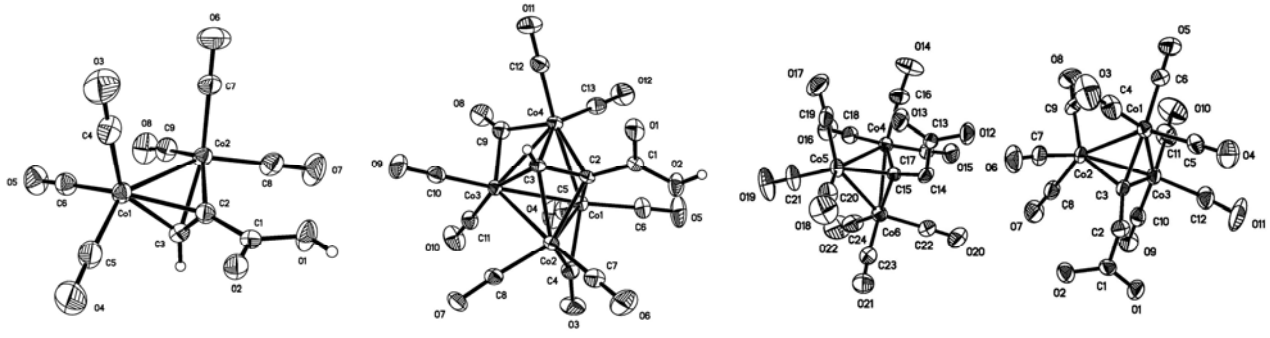

(a) (b) (c)

Fig. 1. Molecular structures of $Co_2(CO)_6HCCCOOH$ (a), $Co_4(CO)_{10}HCCCOOH$ (b), and $Co_3(CO)_9CCH_2COOH$ (c).

Table 2
Bond lengths and angles of $Co_3(CO)_9CCH_2COOH$.

Bond lengths (Å)			
Co(1)-Co(2)	2.4595(13)	Co(4)-Co(5)	2.4624(14)
Co(1)-Co(3)	2.4663(13)	Co(4)-Co(6)	2.4631(14)
Co(2)-Co(3)	2.4692(13)	Co(5)-Co(6)	2.4762(15)
Bond angles (°)			
C(4)-Co(1)-Co(2)	93.9(3)	C(16)-Co(4)-Co(5)	104.7(3)
C(5)-Co(1)-Co(2)	147.6(3)	C(17)-Co(4)-Co(5)	151.7(3)
C(6)-Co(1)-Co(2)	105.0(3)	C(18)-Co(4)-Co(5)	92.9(3)
C(3)-Co(1)-Co(2)	49.94(19)	C(15)-Co(4)-Co(5)	49.7(2)
C(4)-Co(1)-Co(3)	151.8(3)	C(16)-Co(4)-Co(6)	150.1(3)
C(5)-Co(1)-Co(3)	99.7(3)	C(17)-Co(4)-Co(6)	92.5(3)
C(6)-Co(1)-Co(3)	97.7(3)	C(18)-Co(4)-Co(6)	103.3(3)
C(3)-Co(1)-Co(3)	50.5(2)	C(15)-Co(4)-Co(6)	49.92(19)
Co(2)-Co(1)-Co(3)	60.17(4)	Co(5)-Co(4)-Co(6)	60.36(4)
C(8)-Co(2)-Co(1)	155.6(3)	C(19)-Co(5)-Co(4)	91.9(3)
C(7)-Co(2)-Co(1)	97.7(2)	C(20)-Co(5)-Co(4)	146.0(3)
C(9)-Co(2)-Co(1)	97.3(3)	C(21)-Co(5)-Co(4)	106.3(3)
C(3)-Co(2)-Co(1)	50.14(19)	C(15)-Co(5)-Co(4)	50.5(2)
C(8)-Co(2)-Co(3)	98.9(3)	C(19)-Co(5)-Co(6)	150.7(3)
C(7)-Co(2)-Co(3)	144.6(3)	C(20)-Co(5)-Co(6)	102.8(3)
C(9)-Co(2)-Co(3)	102.3(3)	C(21)-Co(5)-Co(6)	95.5(3)
C(3)-Co(2)-Co(3)	50.5(2)	C(15)-Co(5)-Co(6)	49.78(19)
Co(1)-Co(2)-Co(3)	60.05(4)	Co(4)-Co(5)-Co(6)	59.83(4)
C(12)-Co(3)-Co(1)	96.9(3)	C(22)-Co(6)-Co(4)	99.5(3)
C(10)-Co(3)-Co(1)	152.8(2)	C(23)-Co(6)-Co(4)	149.7(3)
C(11)-Co(3)-Co(1)	98.8(3)	C(24)-Co(6)-Co(4)	97.4(3)
C(3)-Co(3)-Co(1)	49.89(19)	C(15)-Co(6)-Co(4)	50.5(2)
C(12)-Co(3)-Co(2)	147.6(3)	C(22)-Co(6)-Co(5)	145.6(3)
C(10)-Co(3)-Co(2)	97.2(2)	C(23)-Co(6)-Co(5)	93.4(3)
C(11)-Co(3)-Co(2)	102.0(3)	C(24)-Co(6)-Co(5)	105.1(3)
C(3)-Co(3)-Co(2)	49.66(19)	C(15)-Co(6)-Co(5)	49.5(2)
Co(1)-Co(3)-Co(2)	59.78(4)	Co(4)-Co(6)-Co(5)	59.80(4)

Symmetry transformations used to generate equivalent atoms.

numbers less than 5 were analyzed using a Porapak Q column and an FID detector.

2.5. Catalyst characterization

Infrared (IR) spectra were recorded on a NEXUS-670 FT-IR spectrophotometer using KBr pellets. Thermogravimetric (TG) analysis in the range 25–600 °C (10 °C/min) was recorded under Ar (30 mL/min) on a Netzsch apparatus, Model STA 449. Co contents were measured using a Varian ICP-AES spectrometer. BET surface areas and pore structure were measured using a Micromeritics ASAP 2020 analyzer using N_2 adsorption at –196 °C. Transmission electron microscopy (TEM) investigations were carried out using a JEOL JEM-2010 (200 kV) transmission electron microscope. NH_3 temperature-programmed desorption (NH_3-TPD) was performed with a quartz tube. The activating treatment was at 550 °C for 30 min under Ar. The NH_3 temperature-programmed desorption was subsequently performed from 120 to 550 °C.

3. Results and discussion

3.1. F-T synthesis

The activity and selectivity of the Co/Al_2O_3 catalysts for F-T synthesis are shown in Table 3. CO conversion and C_{5+} selectivity of the Co_n/γ-Al_2O_3 catalysts were significantly higher than that of the $Co(N)/\gamma$-Al_2O_3 catalyst. Co_3/γ-Al_2O_3 showed the highest C_{5+} selectivity and CO conversion of 79.7% and 89.2%, respectively, while CH_4 and CO_2 selectivity was decreased to 16.6% and 2.8%. The order of CO conversion and C_{5+} selectivity over the catalysts was Co_3/γ-Al_2O_3 > Co_2/γ-Al_2O_3 > Co_4/γ-Al_2O_3 > $Co(N)/\gamma$-Al_2O_3. Figure 2 shows the changes of CO conversion and C_{5+} selectivity with time on stream for the Co_n/γ-Al_2O_3 and $Co(N)/\gamma$-Al_2O_3 catalysts. CO conversion and C_{5+} selectivity decreased to varying degrees with time.

Table 3
Performance of the Co-based catalysts in F-T synthesis.

Catalyst	CO conversion (%)	Product selectivity (%)			
		CH_4	C_2–C_4	CO_2	C_{5+}
Co_2/γ-Al_2O_3	88.2	19.7	0.6	3.3	76.4
Co_3/γ-Al_2O_3	89.2	16.6	0.4	2.8	79.7
Co_4/γ-Al_2O_3	82.7	20.5	0.9	3.2	75.5
$Co(N)/\gamma$-Al_2O_3	54.1	34.0	1.7	3.4	60.9

Reaction conditions: 220 °C, 2.0 MPa, H_2/CO = 2, GHSV = 500 h^{-1}, 14.5 h.

3.2. IR results

The IR spectra of the $Co_3(CO)_9CCH_2COOH$, γ-Al_2O_3, $Co(N)/\gamma$-Al_2O_3, and Co_3/γ-Al_2O_3 catalysts are presented in Fig. 3. The absorption peaks of Co_3O_4 derived from calcined $Co(N)/\gamma$-Al_2O_3 were at 659 and 571 cm^{-1} [9]. The characteristic absorption peaks of γ-Al_2O_3 appeared at 3420, 1625, 806, and 558 cm^{-1}. The set of bands at 2103, 2042, and 2011 cm^{-1} in the ν_{CO} region and 1663 and 1399 cm^{-1} in ν_{COO^-} region of the

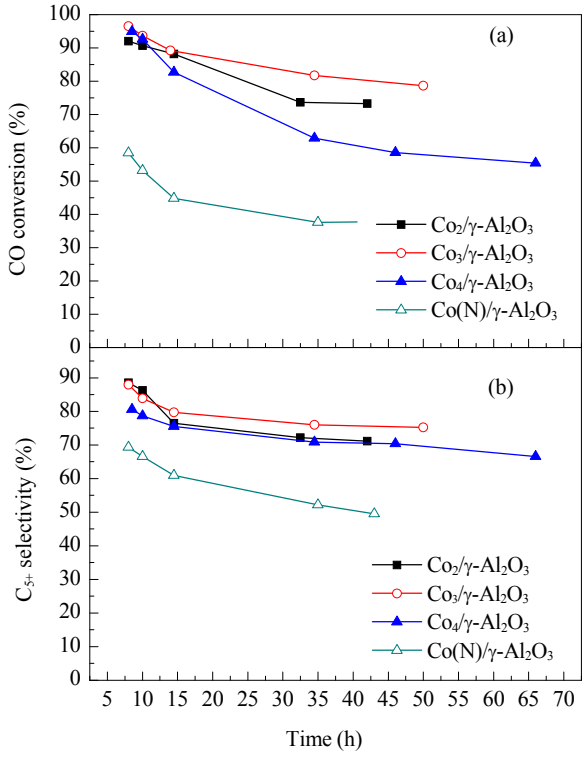

Fig. 2. CO conversion (a) and C_{5+} selectivity (b) with time on stream over different Co-based catalysts.

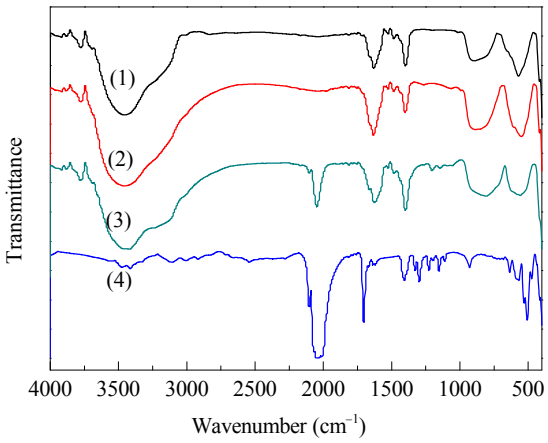

Fig. 3. IR spectra of different samples. (1) Co(N)/γ-Al_2O_3; (2) γ-Al_2O_3; (3) Co_3/γ-Al_2O_3; (4) $Co_3(CO)_9CCH_2COOH$.

$Co_3(CO)_9CCH_2COOH$ precursor represented the signature of the cluster. For the Co_3/γ-Al_2O_3 sample, the profile of the carbonyl and carboxyl group bands remained unchanged, indicating that the supported cluster precursor kept the structural feature of the precursor.

3.3. TG results

Figure 4 shows the TG curve of the $Co_3(CO)_9CCH_2COOH$ precursor. There were two stages of mass loss. The mass loss of 31.65% between 30 and 200 °C at the first stage corresponded to the loss of six carbonyl groups (calculated 33.0%). The next stage from 200 to 360 °C corresponded to the loss of the remaining carbonyl ligands and CO_2 moieties from the carboxyl group (COOH). Loss of part of the terminal carbonyl groups has been reported, and the thermal decomposition of $Co_2(CO)_6HCCCOOH$ and $Co_4(CO)_{10}HCCCOOH$ occurred at 200 °C [8]. The TG analysis indicated that the molecular skeleton of the cobalt carbonyl clusters was stable at 220 °C under an inert atmosphere. The Co atoms, therefore, can be arranged in orderly rows on the support, leading to a higher dispersion of Co on the support.

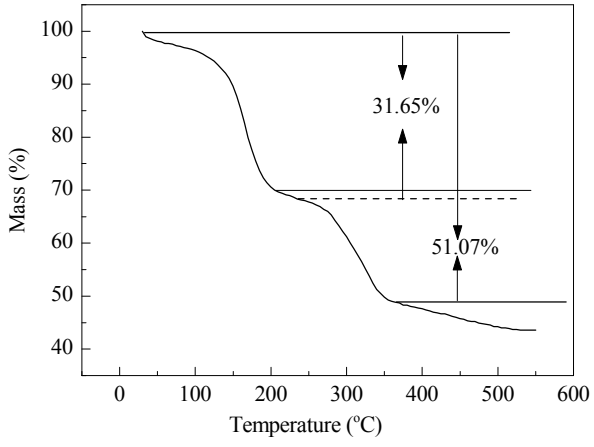

Fig. 4. TG curve of $Co_3(CO)_9CCH_2COOH$.

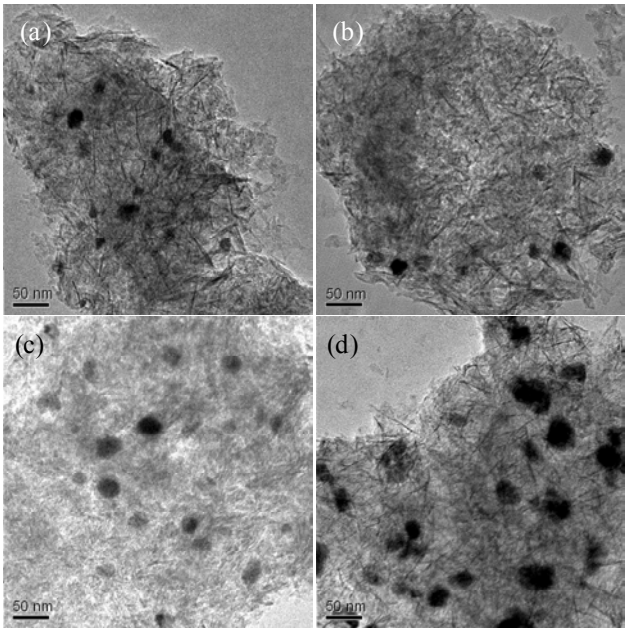

Fig. 5. TEM images of the spent Co-based catalysts. (a) Co_2/γ-Al_2O_3; (b) Co_3/γ-Al_2O_3; (c) Co_4/γ-Al_2O_3; (d) Co(N)/γ-Al_2O_3.

3.4. TEM results

Figure 5 presents the TEM images of the spent Co-based catalysts after reaction for 60 h. The particle size of the Co species in the Co_n/γ-Al_2O_3 catalysts was smaller than that in the Co(N)/γ-Al_2O_3 catalyst, suggesting that the degree of agglomeration on the Co_n/γ-Al_2O_3 catalysts was significantly less than that on the reference catalyst. Since the number of active sites on the catalyst decrease with the increase of Co particle size, the Co_n/γ-Al_2O_3 catalysts would exhibit higher activity than the reference catalyst, which was in good agreement with the results of the catalytic performance measurements.

Table 4 lists Co contents determined by EDS and ICP, where "difference" represents the mass percentage difference in the Co content between the data determined by EDS and ICP. It can be seen that the difference for the Co(N)/γ-Al_2O_3 catalyst was much larger than those for the Co_n/γ-Al_2O_3 catalysts. This indicated that the aggregation of Co on the Co(N)/γ-Al_2O_3 catalyst was much higher than that on the Co_n/γ-Al_2O_3 catalysts. The result suggested that the carboxylic acid ligands of the cobalt carbonyl clusters made the Co species in the Co_n/γ-Al_2O_3 catalysts more uniformly distributed on the support surface during the preparation. The regulating and control of the active metals on the molecular level for the Co_n/γ-Al_2O_3 catalysts gave active metals with smaller particle size and higher dispersion on the

Table 4
Co content of the Co-based catalysts measured by EDS and ICP methods.

Sample	EDS (%)	ICP (%)	Difference (%)
Co_2/γ-Al_2O_3	14.04	7.11	6.93
Co_3/γ-Al_2O_3	13.27	6.98	6.59
Co_4/γ-Al_2O_3	13.64	7.02	6.62
Co(N)/γ-Al_2O_3	30.27	9.02	21.25

support. In addition, the zero valence Co particles of the $Co_n/\gamma\text{-}Al_2O_3$ catalysts without the need for a high temperature pretreatment led to Co particles with less interaction with the support. So the catalysts derived from the Co carbonyl clusters have better dispersion and higher catalytic activity, which explained why the $Co_n/\gamma\text{-}Al_2O_3$ catalysts have higher CO conversion and C_{5+} selectivity [12–14].

3.5. Textural properties

The textural properties of different Co-based catalysts are given in Table 5. The surface area, pore volume, and average pore diameter of the Co-based catalysts were smaller than that of the support, which provided direct evidence that some active species were deposited in the pores of the support. In general, a larger surface area of the catalyst improves F-T catalytic activity, but the surface area of $Co(N)/\gamma\text{-}Al_2O_3$ was almost equal to the surface areas of $Co_n/\gamma\text{-}Al_2O_3$, indicating that the surface area was not a main factor affecting the catalytic activity. However, for the $Co_n/\gamma\text{-}Al_2O_3$ catalysts, the smaller pore size indicated extended residence time of the products in the channel, and slower diffusion of the products in the pores, which is favorable for the re-absorption of α-olefin in the support to give an increase in the selectivity to long chain hydrocarbons. In contrast, the larger pore size of the $Co(N)/\gamma\text{-}Al_2O_3$ catalyst led to faster diffusion of the products, which has a strong influence on the adsorption of CO and H_2 and consequently on the growth of the carbon chain [15]. Therefore, the C_{5+} selectivity of the $Co_n/\gamma\text{-}Al_2O_3$ catalysts were significantly higher than that of the $Co(N)/\gamma\text{-}Al_2O_3$ catalyst.

3.6. NH_3-TPD results

The acidic property of the $Co_n/\gamma\text{-}Al_2O_3$ catalysts was studied by NH_3-TPD (Fig. 6). The results indicated there were three acid sites which were not distributed uniformly on the surface. The two main peaks at 212 and 507 °C were due to the weak acid sites and strong acid sites, respectively, for the $Co_n/\gamma\text{-}Al_2O_3$ catalysts. The desorption peak at 431 °C corresponded to medium strong acid sites of the $Co_3/\gamma\text{-}Al_2O_3$ catalyst and the peaks at 409 and 368 °C were attributed to medium strong acid sites for both the $Co_2/\gamma\text{-}Al_2O_3$ and $Co_4/\gamma\text{-}Al_2O_3$ catalysts. The number of surface acid sites on the $Co_n/\gamma\text{-}Al_2O_3$ catalysts was in the order of $Co_4/\gamma\text{-}Al_2O_3 > Co_2/\gamma\text{-}Al_2O_3 > Co_3/\gamma\text{-}Al_2O_3$, which was consistent with the reverse order of catalytic activity and selectivity of the catalysts for the F-T reaction. This can be explained by that fewer acid sites on the catalyst means less cracking of long chain hydrocarbons on the acid sites, which is favorable for promoting the C_{5+} selectivity [16]. Moreover, fewer strong acid sites led to a decrease of carbon deposition on the support because carbon deposition occurs preferentially on strong acid sites. It is only after the strong acid sites are almost completely covered that carbon would deposit on the weak acid sites [17,18]. Less carbon deposition on the acid sites would be favorable for the activity, which could be another reason for the best catalytic performance of $Co_3/\gamma\text{-}Al_2O_3$ among the three cluster-derived catalysts. More research is needed on the effect of surface acidity on the catalytic activity for the F-T reaction.

Table 5
Textural properties of the support and the catalysts.

Sample	BET surface area (m^2/g)	Pore volume (cm^3/g)	Pore size (nm)
$\gamma\text{-}Al_2O_3$	240.09	0.80	12.7
$Co(N)/\gamma\text{-}Al_2O_3$	198.29	0.67	12.8
$Co_2/\gamma\text{-}Al_2O_3$	200.06	0.55	10.4
$Co_3/\gamma\text{-}Al_2O_3$	180.22	0.55	11.6
$Co_4/\gamma\text{-}Al_2O_3$	209.39	0.55	10.0

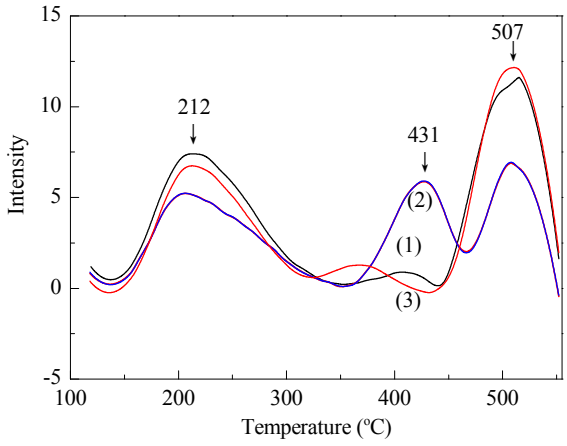

Fig. 6. NH_3-TPD profiles of the Co-based catalysts. (1) $Co_2/\gamma\text{-}Al_2O_3$; (2) $Co_3/\gamma\text{-}Al_2O_3$; (3) $Co_4/\gamma\text{-}Al_2O_3$.

4. Conclusions

A series of $Co/\gamma\text{-}Al_2O_3$ were prepared using cobalt carbonyl clusters and $Co(NO_3)_2$ as precursors. The dispersion of the metallic cobalt species derived from the cobalt carbonyl clusters was better than that prepared with $Co(NO_3)_2$, which resulted in better catalytic behavior in the F-T reaction. The structures of the cobalt carbonyl clusters gave catalysts with different surface acidities. The $Co_3/\gamma\text{-}Al_2O_3$ catalyst with less acid sites gave higher CO conversion and C_{5+} selectivity than the $Co_2/\gamma\text{-}Al_2O_3$ and $Co_4/\gamma\text{-}Al_2O_3$ catalysts.

References

[1] Shu G P, Shi S D, Li K J. Coal Liquefaction Technology. Beijing: China Coal Industry Publishing House, 2003. 186
[2] Puskas I, Hurlbut R S. *Catal Today*, 2003, 84: 99
[3] Iglesia E, Reyes S C, Madon R J. *J Catal*, 1991, 129: 238
[4] Wei M D, Okabe K, Arakava H, Teraoka Y. *New J Chem*, 2003, 27: 928
[5] Matsuzaki T, Hanaoka T-a, Takeuchi K, Arakawa H, Sugi Y, We K M, Dong T L, Reinikainen M. *Catal Today*, 1997, 36: 311
[6] Kraum M, Baerns M. *Appl Catal A*, 1999, 186: 189
[7] Niemelä M K, Krause A O I, Vaara T, Kiviaho J J, Reinikainen M K O. *Appl Catal A*, 1996, 147: 325
[8] Calvo-Perez V, Vega C A, Cortes P, Spodine E. *Inorg Chim Acta*, 2002, 333: 15
[9] Sexton B A, Hughes A E, Turney T W. *J Catal*, 1986, 97: 390
[10] Viswanathan B, Gopalakrishnan R. *J Catal*, 1986, 99: 342

Graphical Abstract

Chin. J. Catal., 2014, 35: 342–350 doi: 10.1016/S1872-2067(12)60757-8

Cobalt-based catalysts derived from cobalt carbonyl clusters for Fischer-Tropsch synthesis

Xuefen Li, Fenghua Bai, Haiquan Su *
Inner Mongolia University

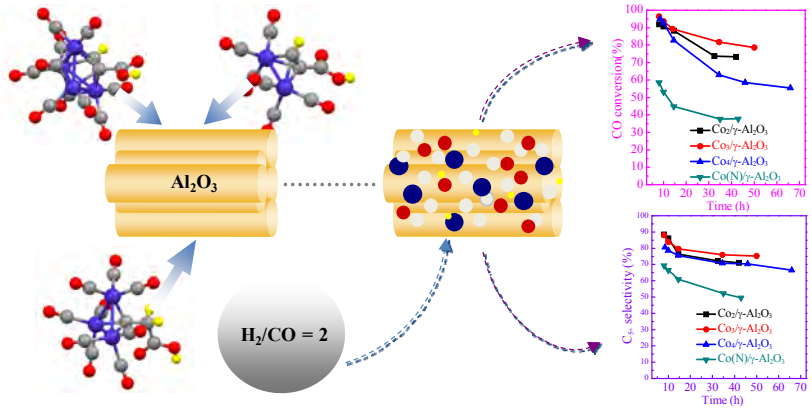

A series of Co-based catalysts supported on γ-Al_2O_3 prepared using cobalt carbonyl clusters showed higher CO conversion and C_{5+} selectivity in F-T synthesis than a reference catalyst prepared using $Co(NO_3)_2$.

[11] Dai X P, Yu C C, Shen S K. *Chin J Catal* (代小平, 余长春, 沈师孔. 催化学报), 2000, 21: 161
[12] Mirzaei A A, Faizi M, Habibpour R. *Appl Catal A*, 2006, 306: 98
[13] Bian G Z, Mochizuki T, Fujishita N, Nomoto H, Yamada M. *Energy Fuels*, 2003, 17: 799
[14] Ma W P, Ding Y J, Lin LW. *Ind Eng Chem Res*, 2004, 43: 2391
[15] Yin Y G. Research Methods of Heterogeneous Catalysts. Beijing: Chemical Industry Press, 1988: 34
[16] Chen X W. [PhD dissertation]. Dalian: Dalian Univ Technol, 2009. 46
[17] Guo C L, Fang X C, Jia L M, Liu Q J. *Petrol Processing Petrochem*, 2012, 43(4): 25
[18] Pan L R, Jia C J, Li H X. *Chin J Catal* (潘履让, 贾春娟, 李赫喧. 催化学报), 1989, 10: 372

以钴羰基簇合物为前驱体制备的钴基催化剂上F-T反应性能

李雪芬[a], 白凤华[b], 苏海全[a,b,*]
[a]内蒙古大学生命科学学院, 内蒙古呼和浩特010021
[b]内蒙古大学化学化工学院, 内蒙古呼和浩特010021

摘要: 以含羧酸配体的钴羰基簇合物$Co_2(CO)_6HCCCOOH$, $Co_3(CO)_9CCH_2COOH$, $Co_4(CO)_{10}HCCCOOH$ 为前驱体, γ-Al_2O_3为载体, 通过浸渍法制备了一系列催化剂; 同时以$Co(NO_3)_2$作为前驱体制备了参比催化剂. 对制备的催化剂进行了费托反应性能评价, 并用透射电子显微镜、氨程序升温脱附和傅里叶变换红外光谱等手段对催化剂进行了表征. 结果发现, 不同前驱体制备的催化剂对载体上Co的分布具有明显影响, 进而影响催化剂活性. 反应结果表明, 不同前驱体制备的催化剂上CO转化率及C_{5+}选择性顺序为$Co_3(CO)_9CCH_2COOH > Co_2(CO)_6HCCCOOH > Co_4(CO)_{10}HCCCOOH > Co(NO_3)_2$.

关键词: 钴羰基簇合物; 费托合成; 前驱体; 浸渍法

收稿日期: 2013-09-02. 接受日期: 2013-11-22. 出版日期: 2014-03-20.
*通讯联系人. 电话/传真: (0471)4992981; 电子信箱: haiquansu@yahoo.com
基金来源: 国家自然科学基金(21061008); 内蒙古自然科学基金重大项目(2010ZD01).
本文的英文电子版由Elsevier出版社在ScienceDirect上出版(http://www.sciencedirect.com/science/journal/18722067).

1. 前言

Fischer-Tropsch合成(F-T合成)是将煤或天然气转化为洁净液体燃料的有效途径. 钴基催化剂由于具有高的催化CO加氢活性和链增长能力, 反应过程中稳定且不易积炭和中毒等优点而成为F-T合成中最有发展前途的催化剂[1]. F-T合成烃类产物一般服从ASF分布, 难以高选择性地得到某一油品, 因此提高C_{5+}选择性、抑制甲烷等副产物的生成成为研究F-T合成新型钴基催化剂的关键问题[2,3]. 许多研究表明, 用浸渍法制备负载型Co基催

化剂时, 钴源对金属-载体相互作用、Co的分散度和还原性有显著的影响, 进而影响催化剂的活性和选择性[4,5]. 常用的钴源除了硝酸钴等无机盐外, 还有羰基钴(如$Co_2(CO)_8$和$Co_4(CO)_{12}$)、Co-EDTA配合物、乙酰丙酮钴配合物及乙酸钴等有机钴化合物. Kraum等[6]系统地研究了不同钴源对Co/TiO_2催化剂性能的影响, 发现各催化剂F-T反应活性顺序为: $Co(COO)_2$ > $Co(CH_3COO)_2$ > $Co(acac)_3$ > $Co(NO_3)_2$ > Co-EDTA> $Co(acac)_2$; Niemelä等[7]报道, 用不同钴源制备的5%Co/SiO_2催化剂, 金属Co的分散性顺序为: $Co_2(CO)_8$ > $Co_4(CO)_{12}$ >> $Co(NO_3)_2$. 研究普遍认为, F-T反应催化活性中心是零价金属粒子, 因此以钴盐为前驱体制备的催化剂, 需用H_2高温还原, 而羰基钴簇合物中的金属钴以零价态形式存在, 可在较低的温度下得到金属粒子, 同时簇合物的多金属协同作用在F-T催化反应中也具有潜在的应用价值. 本文以含有羧酸配体的钴羰基簇合物为前驱体制备了一系列催化剂, 用于F-T反应中, 并与$Co(NO_3)_2$为前驱体的催化剂性能进行了比较.

2. 实验部分

2.1. 材料与试剂

$Co(NO_3)_2·6H_2O$为国产分析纯, γ-Al_2O_3为Alfa Aesar产品. $Co_4(CO)_{10}HCCCOOH$与$Co_2(CO)_6HCCCOOH$参照文献[8]合成, 其分子结构示于图1. $Co_3(CO)_9CCH_2COOH$通过$Co_4(CO)_{10}HCCCOOH$与 $Eu(OOCCF_3)_3$在四氢呋喃(THF)溶剂中反应制得, 所得晶体学参数列于表1, 部分键长键角列于表2中, 分子结构见图1(c). 配合物$Co_3(CO)_9CCH_2COOH$结晶为三斜晶系, 属于P-$\bar{1}$空间群.

2.2. 催化剂的制备

采用等体积浸渍法制备催化剂. 将γ-Al_2O_3载体于500 °C焙烧10 h进行活化和除杂, 之后研磨、筛选40–60目的颗粒. 取一定量γ-Al_2O_3颗粒, 滴加THF至初湿, 记下消耗溶剂的体积, 按照钴的负载量为10 wt%计算出钴羰基簇合物浸渍液的浓度. 将前驱体放入Schleck瓶中, 在N_2气保护下滴加THF至计算量, 待前驱体充分溶解后, 将γ-Al_2O_3浸于其中, N_2保护下于0 ºC浸渍10 h后, 室温下N_2低速吹扫24 h, THF全部挥发后即制得催化剂Co_2/γ-Al_2O_3 (以$Co_2(CO)_6HCCCOOH$为前驱体), Co_3/γ-Al_2O_3 (以$Co_3(CO)_9CCH_2COOH$为前驱体)和Co_4/γ-Al_2O_3 (以$Co_4(CO)_{10}HCCCOOH$为前驱体).

另取一定量载体, 按照10%钴的负载量以$Co(NO_3)_2·6H_2O$溶液浸渍至初润, 静置24 h, 使其活性组分通过毛细作用负载于载体上, 于120 ºC干燥后350 ºC煅烧6 h, 即制得标准催化剂, 记为Co(N)/γ-Al_2O_3.

2.3. 催化剂预处理条件

以不同钴源为前驱体制备催化剂的预处理条件也有所不同, 具体表现为氢气还原温度不同. 采用H_2-TPR手段对Co(N)/γ-Al_2O_3催化剂的还原行为进行分析, 在347和396–470 ºC出现两个还原峰, 分别对应于Co^{3+}→Co^{2+}→Co^0的分步还原[9,10]. 由于在较高温度下Co_3O_4易与氧化铝载体相互作用生成难还原物种$CoAlO_4$尖晶石而导致催化剂活性降低[11], 因此选择Co(N)/γ-Al_2O_3在400 ºC下用氢气还原. Co_n/γ-Al_2O_3 (n = 2, 3, 4; 下同)催化剂中Co为零价, 仅需在200 ºC用H_2吹扫.

2.4. 催化剂的评价

F-T反应在加压固定床反应器(ϕ 18 mm × 700 mm)中进行. 催化剂装填量为4 g, 催化剂在常压、200 ºC (Co(N)/γ-Al_2O_3在400 ºC下以纯氢气吹扫10 h , 自然降温至180 ºC后切换为合成气(H_2/CO = 2), 升压至2.0 MPa, 在60 min内升温至220 ºC. F-T反应条件: T = 220 ºC, p = 2.0 MPa, H_2/CO = 2, GHSV = 500 h^{-1}. 经脱氧、脱水和脱硫等净化处理的原料气由质量流量计控制进气, 湿式流量计计量后放空. 尾气中的H_2, CO, CH_4及CO_2由装碳分子筛柱TDX-01的Shimadzu公司GC-8APT型气相色谱进行分析, TCD检测; 尾气中的CH_4和C_2, C_3, C_4等烃类由Propack-Q固定相色谱柱分析, FID检测器. 反应达到稳态后, 每隔2 h采样一次. 对气相的分析数据进行归一, 得到CO转化率、CH_4选择性、CO_2选择性、C_2–C_4选择性及C_{5+}选择性.

2.5. 催化剂的表征

红外光谱(IR)用NEXUS-670型红外光谱仪(KBr压片)测定, 记录范围4000–400 cm^{-1}. 热重分析(TG)采用德国NETZSCH公司STA 449C型差热-热重联用分析仪测定, Ar气氛(30 mL/min)中以10 ºC/min从25升至600 ºC. ICP化学分析采用四酸(HCl, HNO_3, HF和$HClO_4$)消解法将样品配成一定浓度的溶液, 之后用美国Varian ICP-AES光谱仪测定溶液中的Co含量. 比表面积及孔结构测试使用美国Micromeritics ASAP 2020型物理吸附仪进行测定. 采用容量法, 在–196 °C下以氮(99.99%)为吸附质进行测试. 透射电子显微镜(TEM)测试使用日本电子株式会社JEOL JEM-2010透射电子显微镜, 加速电压为200 kV. NH_3 程序升温脱附(NH_3-TPD)在石英反应管中进行, 样品先于550 ºC在Ar中预处理30 min, 然后降至120 ºC, 通入NH_3至吸附饱和, 再以10 ºC/min程序升温脱

附至550 ºC.

3. 结果与讨论

3.1. F-T反应性能

表3及图2为不同催化剂上的F-T反应性能. 可以看出, Co_n/γ-Al_2O_3催化剂上CO转化率及C_{5+}选择性明显高于Co(N)/γ-Al_2O_3催化剂, 其中Co_3/γ-Al_2O_3的F-T反应性能最优, CO转化率与C_{5+}选择性分别为89.2%和79.7%, CH_4和CO_2选择性则分别降低至16.6%和2.8%. 不同催化剂上CO转化率及C_{5+}选择性顺序一致: Co_3/γ-Al_2O_3 > Co_2/γ-Al_2O_3 > Co_4/γ-Al_2O_3 > Co(N)/γ-Al_2O_3. 随反应时间的延长, 催化剂上CO转化率及C_{5+}选择性均有所降低.

3.2. IR结果

图3为含羧酸配体的钴羰基簇合物、相应Co/γ-Al_2O_3催化剂及载体的红外光谱. 由于Co_n/γ-Al_2O_3催化剂与前驱体钴羰基簇合物的FT-IR谱相似, 因此只给出Co_3/γ-Al_2O_3. 由图3可见, Co(N)/γ-Al_2O_3样品在659和571 cm^{-1}处出现Co_3O_4的特征吸收峰($Co(NO_3)_2{\cdot}6H_2O$在350 ºC煅烧后分解为Co_3O_4[9]); Co_3/γ-Al_2O_3与$Co_3(CO)_9CCH_2COOH$样品特征峰一致: 2103和2042 cm^{-1}为端羰基伸缩振动峰, 1663和1399 cm^{-1}为羧基伸缩振动峰, 3420, 1625, 806和558 cm^{-1}处为γ-Al_2O_3的特征吸收峰. 可见, 前驱体通过浸渍法引入到载体的表面或孔穴中, 其骨架结构得以保持.

3.3. TG结果

图4为催化剂前驱体$Co_3(CO)_9CCH_2COOH$的TG曲线. 可以看出, 该样品热分解分为三个阶段: (1) 30–200 ºC, 前驱体部分端羰基配体以CO气体的形式脱掉, 且随着温度的升高而变得剧烈; (2) 200–360 ºC, 对应于剩余的羰基配体和以CO_2形式分解掉的羧基配体的脱除; (3) 360 ºC后分解变得缓慢, 趋于平稳. 在反应温度(220 ºC时), 该前驱体失重31.65%, 认为失去6个端羰基(理论值33%). 同样地, Víctor等[8]对簇合物$Co_2(CO)_6HCCCOOH$及$Co_4(CO)_{10}HCCCOOH$进行TG分析后认为, 在200 ºC时, 两种簇合物分解仅失去端羰基. 通过热稳定性分析发现, 在惰性气氛下及220 ºC的活化温度下, 含羧酸配体的钴羰基簇合物脱去羰基而形成活性组分钴. 由于簇合物仍保留着分子骨架, 使其活性中心钴原子可以有序地排列在载体上, 从而保持较好的分散性.

3.4. TEM结果

图5为催化剂在220 ºC反应60 h后的TEM照片. 可以看到, 以传统方法制备的Co(N)/γ-Al_2O_3催化剂在F-T反应后, 大量的Co晶粒团聚形成大的Co金属颗粒, 减少了活性位Co的数目; 而以不同钴核数羰基簇合物为前驱体的催化剂Co_n/γ-Al_2O_3, 在反应后团聚的程度明显变小, 在载体表面的分散度较高.

表4列出了SEM-EDS和ICP测得的Co含量. 由表可见, 通过两种方法测得Co(N)/γ-Al_2O_3催化剂钴含量的差值远远大于Co_n/γ-Al_2O_3催化剂的, 同样说明在催化反应过程中, Co(N)/γ-Al_2O_3中的活性钴原子团聚程度远高于Co_n/γ-Al_2O_3催化剂中原子的团聚. 在制备Co_n/γ-Al_2O_3催化剂过程中, 含羧酸配体的钴羰基簇合物通过有机配体骨架使活性中心Co在载体表面均匀分布, 这种分子水平上对活性金属的调控使其具有较小的颗粒尺寸和较高的分散度, 并且负载后的钴以零价态形式存在, 无需高温还原即可使用, 因而降低了金属钴与载体之间的相互作用, 从而获得较好的分散度和较高的活性位. 因此, 与Co(N)/γ-Al_2O_3相比, Co_n/γ-Al_2O_3催化剂具有较高的CO转化率及C_{5+}选择性[12–14].

3.5. 织构性质

表5为各样品的织构性质. 由表可见, 前驱体的负载使得相应样品的比表面积、孔体积和孔径均有所减小, 表明催化剂前驱体在载体表面聚集并部分进入载体孔道. 一般而言, 催化剂的比表面积越大越有利于提高F-T催化活性, 但Co(N)/γ-Al_2O_3与Co_n/γ-Al_2O_3的比表面相差不多, 说明比表面积并不是影响F-T催化活性的主要因素.

还可以看出, Co_n/γ-Al_2O_3催化剂的平均孔径要小于Co(N)/γ-Al_2O_3催化剂. 催化剂孔径减小, 可使形成的产物在孔道内停留时间增加, 孔道内产物扩散减慢, 有利于α-烯烃的再吸附, 从而增加重质烃的选择性; 而较大的孔径使生成产物容易脱附, 不利于α-烯烃的再吸附, 不但阻止了碳链的增长而且不利于CO和H_2的扩散和吸附, 使反应速率降低[15]. 因此, 具有更多小孔径分布的Co_n/γ-Al_2O_3催化剂具有更高的催化活性及C_{5+}选择性.

3.6. NH_3-TPD结果

图6为Co_n/γ-Al_2O_3催化剂的NH_3-TPD谱. 由图可见, Co_n/γ-Al_2O_3催化剂表面酸性强度分布很不均匀, 具有三个酸性中心. 三个配合物在212和507 ºC左右的脱附谱峰形一致, 分别对应弱酸中心与强酸中心. Co_3/γ-Al_2O_3催化剂在431 ºC附近有一个明显的脱附温度峰, 对应中强酸中心. Co_2/γ-Al_2O_3和Co_4/γ-Al_2O_3催化剂的中强酸中心分别在409和368 ºC附近. 可以看出, 与Co_2/γ-Al_2O_3和Co_4/γ-Al_2O_3催化剂相比, Co_3/γ-Al_2O_3催化剂的强酸和弱

酸中心强度减小, 而中强酸中心强度增大, 各催化剂酸性位数目顺序为$Co_4/\gamma\text{-}Al_2O_3 > Co_2/\gamma\text{-}Al_2O_3 > Co_3/\gamma\text{-}Al_2O_3$. 结合反应数据可以看出, 催化剂酸性位数目越少, F-T反应活性和C_{5+}选择性越高, 这可能是由于催化剂酸量的减少, 限制了在酸位上长链烃类催化裂解反应的发生, 有利于提高F-T合成反应长链烃选择性[16]. 另外, 由于积炭现象优先发生在强酸活性中心上, 当强酸中心几乎被完全覆盖时, 积炭才开始在弱酸中心上沉积[17,18], 因此$Co_3/\gamma\text{-}Al_2O_3$催化剂F-T反应性能最优也可能是由于强酸性位数目少, 抑制了积炭, 从而提高了F-T反应活性和稳定性. 催化剂酸性对F-T反应活性的影响还有待进一步深入研究.

4. 结论

以含羧酸配体的钴簇基簇合物及无机盐$Co(NO_3)_2$两种不同形式的钴源作为前驱体, $\gamma\text{-}Al_2O_3$为载体, 采用浸渍法制备了一系列F-T合成反应催化剂. 结果表明, 以含羧酸配体的钴簇基簇合物为前驱体制备的催化剂上Co活性中心在载体表面具有较好的分散性, 经过F-T反应后金属粒子团聚程度低于参比催化剂, 进而影响催化剂的活性和选择性. 另外, 空间结构不同导致了簇合物为前驱体的催化剂表面的酸性不同, 酸性位少的$Co_3/\gamma\text{-}Al_2O_3$催化剂上CO转化率及$C_{5+}$选择性明显高于$Co_2/\gamma\text{-}Al_2O_3$及$Co_4/\gamma\text{-}Al_2O_3$催化剂.